Packing in Amorphous Regions of Hydrofluoric-Acid-Doped Polyaniline Powder by $^{15}N-^{19}F$ REDOR NMR

Matthew P. Espe,[†,§] B. R. Mattes,[‡] and Jacob Schaefer*[,†]

Department of Chemistry, Washington University, St. Louis, Missouri 63130, and Los Alamos National Laboratory, Los Alamos, New Mexico 87545

Received May 28, 1997; Revised Manuscript Received July 25, 1997[⊗]

ABSTRACT: Anhydrous ^{15}N-labeled polyaniline powders have been examined by ^{13}C, ^{15}N, and ^{19}F solid-state NMR as a function of HF doping. Chemical shifts in the ^{19}F NMR spectra of doped polyaniline reveal three distinct types of charged environments. Carbon, nitrogen, and fluorine spin counts show that only about one-third of all the chains in fully HF-doped polyaniline are detected. This observation is consistent with the assumption that the entire crystalline region, and amorphous regions within 50 Å of the crystalline border, is rendered unobservable by paramagnetic delocalized electrons in the crystalline region. Rotational-echo double-resonance ^{15}N NMR (with ^{19}F dephasing) indicates that in the observable amorphous regions the polyaniline chains are tightly packed with an in-plane interchain separation of 10 Å and that fully charged main-chain nitrogens have, on average, one nearest-neighbor fluorine 4 Å away and three next-nearest-neighbor fluorines with an average $^{15}N-^{19}F$ distance of just over 5 Å.

Polyaniline is a conducting organic polymer which is transformed from an insulating to a conducting state on doping with protic acids.[1] The repeat unit of the undoped polymer (emeraldine base) has been shown by solid-state ^{13}C NMR to consist of a copolymer of reduced and oxidized bases in which two amine backbone nitrogens alternate with two imine backbone nitrogens.[2] Partial doping of polyaniline (less than two acid molecules per repeat unit) yields mostly dications, whereas full doping results in the presence of dications, cation radicals, and delocalized electron density.[3−5] Both doped and undoped polyanilines can be processed using conventional technology to produce fibers and films with practical applications.[6] The physical properties of polyaniline films in particular are altered by doping and undoping.[7] These properties include electrical conductivity, crystallinity, density, surface area, and tensile strength. In addition, the permselectivity of polyaniline films used for O_2-N_2 gas separations is extremely sensitive to doping history.[8] Unlike electrical conductivity, which depends on chain ordering leading to a three-dimensional, crystalline metallic-like state, gas transport is thought to depend on the morphology and packing of noncrystalline regions.[9] In this paper, we report the use of ^{15}N rotational-echo double resonance (REDOR)[10] with ^{19}F dephasing to characterize the amorphous regions of anhydrous ^{15}N-labeled polyanilines doped by HF.

Experiments

Synthesis of Polyaniline Powder in the Emeraldine Oxidation State. A solution (1 N) in HCl was prepared by adding 85 mL of 38% HCl to 1 L of distilled deionized water. A 128 mL aliquot of this acid solution was placed in a 500 mL polymerization vessel along with 5 g of distilled [^{15}N]aniline (99 atom % ^{15}N, Isotec, Inc., Miamisburg). The mixture was stirred at 273 K. A 116 mL aliquot of 1 N HCl was combined with 4.53 g (0.199 mol) of ammonium peroxydisulfate in a separate flask. This mixture was stirred until all of the oxidant dissolved. The flask was then cooled to 273 K. The persulfate solution was slowly added dropwise to the aniline solution by means of an addition funnel over the course of 30 min. The combined solutions were allowed to react for an additional 3.5 h at 273 K. The green precipitated emeraldine hydrochloride was collected on filter paper in a large Büchner funnel. The powder was extracted first with water and then with methanol, until the wash solutions were colorless, and then the solution was refiltered. This as-synthesized polyemeraldine hydrochloride salt was subsequently immersed in 2 L of 0.1 N ammonium hydroxide for 2 h, filtered, and then washed again with tetrahydrofuran and methanol until the wash solutions were colorless. The yield was 32%. The purified emeraldine base was vacuum-dried (at less than 1×10^{-3} Torr) and stored in a vacuum desiccator.

A 1 N solution in HF was prepared by adding distilled deionized water to 70 mL of 48% HF acid in a 2 L volumetric flask. The final concentration was determined by KOH titration. Additional 0.1 and 0.01 N HF solutions were prepared by dilution. Approximately 500 mg of emeraldine base was added to 1 L of each of the three HF solutions and equilibrated with stirring for 4 days at room temperature. Four-point probe dc conductivity measurements of the resulting HF-doped, vacuum-dried, and pressed emeraldine base powders yielded conductivities of 0.9, 0.09, and 0.001 S/cm, respectively. By comparison to conductivities of HCl-doped polyanilines,[6] doping for the three samples was estimated at 100%, 40%, and 10%, respectively.

Samples for examination by NMR were pumped under dynamic vacuum for 3 days and sealed under vacuum. The samples were pressed into pellets and loaded into zirconia rotors under an inert atmosphere in a glovebox. The rotors were sealed with multivein, gastight Kel-F plugs and stored in the glovebox when not in use.

NMR Spectrometer. Cross-polarization, magic-angle spinning, Hahn-echo ^{13}C, ^{15}N, and ^{19}F NMR spectra were obtained at room temperature using a superconducting solenoid operating at 4.7 T. The single, 9 mm diameter, radio-frequency coil was connected by a low-loss transmission line[11] to a quadruple-resonance tuning circuit,[12] which permits ^{1}H, ^{19}F, ^{13}C, and ^{15}N detection or dephasing at 200, 188, 50, and 20 MHz, respectively. Proton−carbon and proton−fluorine cross-polarization transfers were performed in 1 ms at 50 kHz, followed by proton dipolar decoupling at 90 kHz. Proton−nitrogen transfers were made in 1.5 ms at 50 kHz. Radio-frequency field amplitudes were under active control (±200 Hz). The magic-angle stators were obtained from Chemagnetics (Fort Collins, CO). High-performance 7.5 mm o.d. zirconia rotors were fitted with airtight plastic (Kel-F) end and drive caps and supported at both ends by air-pumped journal bearings.

[†] Washington University.
[‡] Los Alamos National Laboratory.
[§] Present address: Department of Chemistry, University of Akron, Akron, OH 44325.
[⊗] Abstract published in *Advance ACS Abstracts,* September 15, 1997.

S0024-9297(97)00742-0 CCC: $14.00

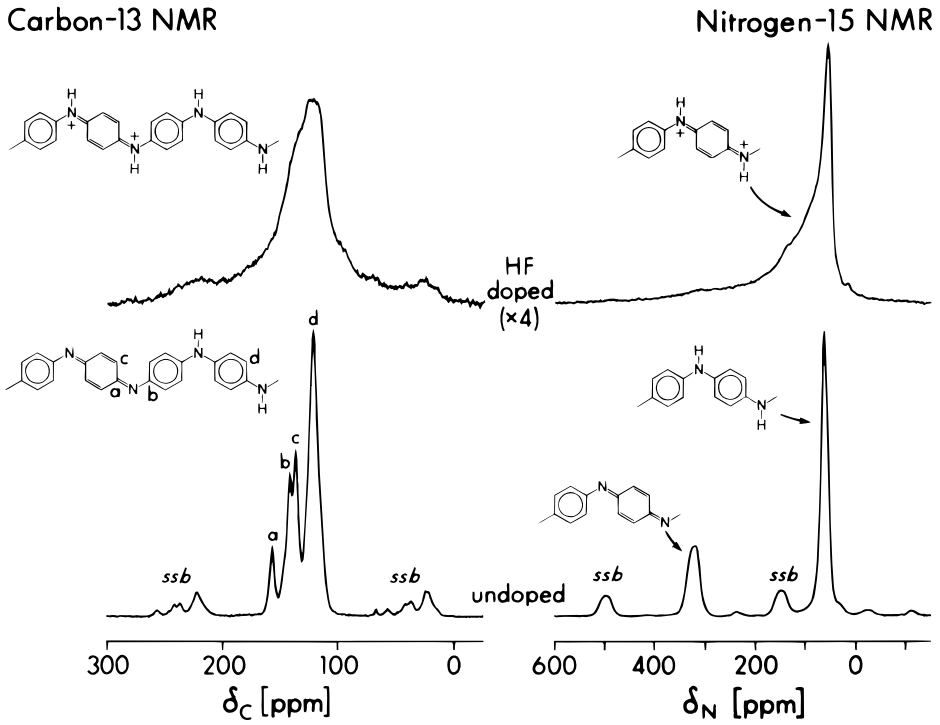

Figure 1. Cross-polarization magic-angle spinning ^{13}C NMR (left) and ^{15}N NMR (right) of HF-doped (top) and undoped (bottom) ^{15}N-labeled polyaniline. The ^{13}C and ^{15}N chemical-shift scales are referenced to external tetramethysilane and solid ammonium sulfate, respectively. Spinning sidebands are designated "ssb". Magic-angle spinning was at 5000 Hz for the ^{13}C NMR spectra and 3520 Hz for the ^{15}N NMR spectra.

REDOR. The pulse sequence for these rotational-echo double-resonance (REDOR) experiments[10] used XY8 π-pulse phase cycling for both ^{15}N and ^{19}F channels. In the absence of any ^{19}F pulses, the echo that formed resulted in S_0, the REDOR full-echo spectrum. Application of phase-alternated[13] fluorine π pulses every half rotor cycle caused a net dephasing of the transverse magnetization of those nitrogens dipolar-coupled to ^{19}F. The resulting spectrum, S, was diminished in intensity. The REDOR difference spectrum ($\Delta S = S_0 - S$) arose only from those nitrogens that were dipolar-coupled to fluorine. REDOR dephasing was accumulated over 8−96 rotor cycles, with magic-angle spinning at 6024 Hz. Because sidebands dephase at a rate different from centerbands,[10] residual spinning sidebands should not be suppressed in REDOR experiments.

DRAMA. Dipolar restoration at the magic angle[14] (DRAMA) uses rotor-synchronized 90° pulses to dephase the magnetization of isolated dipolar-coupled homonuclear spin-$^1/_2$ pair. The full DRAMA sequence[15] used for $^{19}F-^{19}F$ pairs had π pulses at the completion of the odd-numbered rotor cycles to refocus isotropic chemical shifts at the completion of the even-numbered rotor cycles. These π pulses were phase alternated following the XY8 scheme[13] (xyxyyxyx). A complete phase cycle therefore required 16 rotor cycles. The phase of the leading pulse of the XY8 sequence was determined by the ^{19}F-spin quadrature routing.

The frequency-offset dependence of DRAMA due to chemical-shift tensors (and 5 kHz isotropic chemical-shift differences) was removed using eight equally spaced π pulses per rotor cycle.[15] These pulses were placed at 1/16, 3/16, 5/16, etc., of the rotor period (T_r). The phases of these π pulses were also alternated according to the XY8 scheme. Phase accumulation at the spinning frequency and twice the spinning frequency from chemical-shift interactions for transverse magnetization arising from individual crystallites in an isotropic powder cancel under the four sign reversals created in each half rotor cycle by the eight π pulses.[12] Two 90° pulses per rotor period were placed at 1/4 and 3/4 T_r for maximum dephasing. These pulses all had the same phase which was determined by the ^{19}F quadrature routing. The DRAMA-dephased echo that formed at the completion of even numbers of rotor cycles is S. A rotor-synchronized XY8 echo was produced on even-numbered rotor cycles by a refocusing π pulse following the completion of odd-numbered cycles (omitting only the four $\pi/2$ pulses). The DRAMA ^{19}F full echo which formed at the completion of even numbers of rotor cycles is S_0. The ^{19}F DRAMA difference is $\Delta S = S_0 - S$.

SEDRA. Simple excitation for the dephasing of rotational amplitudes (SEDRA) involves the observation of rotational echoes with (S) and without (S_0) rotor-synchronized dephasing.[16] For an isolated $^{19}F-^{19}F$ pair having a significant isotropic shift separation, one π pulse every two rotor periods produces refocusing while one π pulse per rotor period produces dephasing. The phases of the π pulses in these SEDRA experiments followed the XY8 scheme.[13] Therefore, a full echo (S_0) had complete XY8 phase compensation after multiples of 16 rotor cycles, whereas the dephased echo (S) was obtained with full compensation in multiples of 8 rotor cycles. Refocusing was optimized by satisfying the (CEDRA)[17] isotropic chemical-shift separation condition, $\Delta\nu_{iso} = (2n + 1)\nu_r/2$, $n = 1$.

Results

Chemical Shifts. The ^{13}C NMR spectrum of undoped polyaniline has resolved lines for most of the functionally different types of aromatic carbons of the four-ring, main-chain repeat unit (Figure 1, bottom left). The assignments are those cited by Kaplan et al.[2] and Hjertberg et al.[18] A 15.1 MHz ^{13}C dipolar-rotational spin-echo experiment[19] (with magic-angle spinning at 1859 Hz) performed on this material (spectra not shown) gave a ratio of integrated intensities for the second to first dipolar spinning sidebands of 1.04 for the protonated aromatic-carbon line (assignment *d*). This ratio translates[20] into an estimate that 20% of the polyaniline rings are undergoing π flips faster than 10 kHz at 300 K, which is consistent with previous determinations of ring dynamics using ^2H NMR[21] and two-dimensional chemical-exchange experiments.[22] The resolution of the 50 MHz ^{13}C NMR spectrum of ^{15}N-labeled polyaniline is somewhat better than that of a natural-abundance

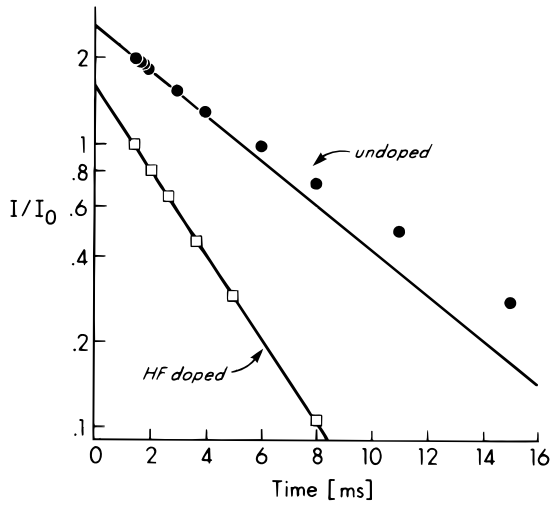

Figure 2. Decay of the spin-locked proton magnetization of HF-doped and -undoped ^{15}N-labeled polyaniline, as monitored by the 67 ppm amine-nitrogen magnetization following a cross-polarization transfer from protons.

emeraldine base because magic-angle spinning completely averages line broadening due to ^{13}C−^{15}N dipolar coupling. Just as observed for fully doped polyaniline hydrochloride,[2,21] all resolution is lost on HF doping (Figure 1, top left), which we attribute to site heterogeneity and a distribution of isotropic chemical shifts.[2,21]

The ^{15}N NMR spectrum of undoped polyaniline has equal integrated intensities for imine nitrogens (320 ppm, Figure 1, bottom right) and amine nitrogens (67 ppm). The imine-nitrogen peak disappears on HF doping[23] and is replaced by a broad distribution of peaks between 80 and 140 ppm, which we assign to positively charged protonated nitrogens (see structure, Figure 1, top right).[24,25] The integrated intensities of both ^{13}C and ^{15}N NMR spectra decrease by about two-thirds following full doping. We attribute this decrease to the presence of unpaired electrons (observed $g = 2.0$, line width of 1.5 G) primarily in the ordered, crystalline regions, which are pseudo-metallic and conducting.[5,26] The local paramagnetism broadens lines in these regions, as well as in adjacent amorphous domains, so that the total magic-angle spinning intensity is diminished. The remaining observed signal therefore arises primarily from amorphous regions or domains more than 50 Å distant from paramagnetic centers.[27] Spin-locked proton magnetization (monitored by the 67 ppm neutral amine-nitrogen peak) shows the disappearance of two-phase behavior[28] on doping (Figure 2), which we attribute to the observation of just an amorphous component. The measurements of Figure 2 (top) only cover one decade of signal intensity and therefore are not suitable to establish unambiguously the long $T_{1\rho}(H)$ and a reliable estimate of the relative concentrations of amorphous and crystalline regions. No Overhauser or solid-effect dynamic nuclear polarization enhancements were observed, which suggests that the unpaired electrons are delocalized.[27]

The ^{19}F NMR spectrum of doped polyaniline reveals three chemical-shift environments, whose relative concentrations vary as a function of doping level (Figure 3). All three environments are present for low concentrations of HF. We assign these peaks to the three possible arrangements of F− counter anions near positively charged nitrogens, in order of most complete fluorine charge to least complete fluorine charge,[29] low magnetic field to high magnetic field, respectively. Details of the

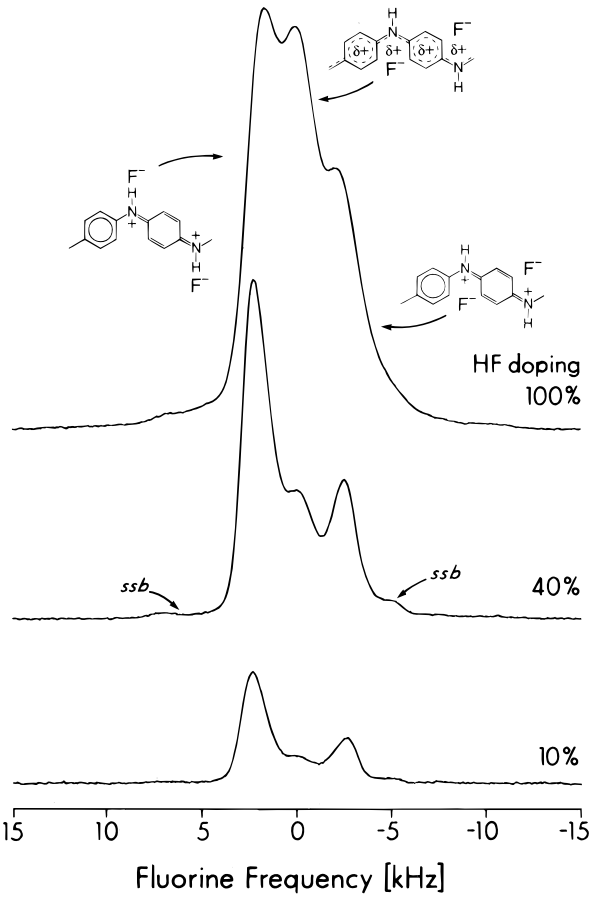

Figure 3. Cross-polarization magic-angle spinning proton-decoupled ^{19}F NMR spectra of ^{15}N-labeled polyaniline as a function of HF doping.

distribution and geometrical arrangements of fluorines in polyaniline hydrofluoride will be considered more fully in the discussion. The ^{19}F spin count also reflects diminished intensity due to an increase in the number of paramagnetic sites in the more highly doped materials. The integrated intensity of the fully HF-doped polyaniline is about five to six times that of the 10% doped material (Figure 3, top and bottom), consistent with the fact that only about 30% of the fully HF-doped polyaniline is observed by ^{19}F NMR.

REDOR, DRAMA, and CEDRA Dephasing. The REDOR ^{15}N NMR full-echo spectrum of fully HF-doped polyaniline (Figure 4, bottom) has components which we assign to fully charged nitrogens (138 ppm), partially charged nitrogens (80 ppm), and uncharged amine nitrogens (56−60 ppm). The REDOR ^{15}N difference spectrum with ^{19}F dephasing (Figure 4, top) is skewed toward low field relative to the full-echo spectrum, which shows stronger dipolar coupling of fluorides to charged nitrogens than to uncharged nitrogens.

The REDOR ^{19}F NMR spectra (with ^{15}N dephasing) of fully doped polyaniline showed that all three lines dephased at about the same rate (spectra not shown). However, the echo-train ^{19}F lifetime of about 3 ms made characterization for large ΔS problematic. The lifetime was increased to only about 5 ms by phase modulation of the decoupling proton radio-frequency field. The 15%−20% DRAMA dephasing of lightly doped polyaniline, after only eight rotor cycles, is significantly greater than the corresponding CEDRA dephasing (Figure 5). This means that for lightly doped polyaniline, the fluorides locate in regions of similar chemical structure. Assuming only ^{19}F−^{19}F pairs are present in

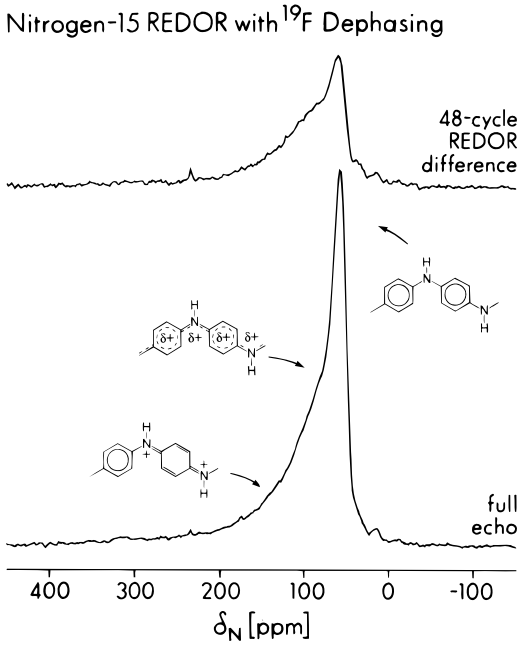

Figure 4. REDOR ^{15}N NMR spectra of fully HF-doped ^{15}N-labeled polyaniline. The full-echo spectrum (after 48 rotor cycles) is shown at the bottom of the figure and the REDOR difference (with ^{19}F dephasing) at the top. Magic-angle spinning was at 6024 Hz.

the lightly doped sample, the observed dephasing corresponds[15] to a fluorine−fluorine distance of about 8 Å.

Discussion

Model for HF-Doped Polyaniline. The complete REDOR dephasing ($\Delta S/S_0$) for ^{15}N magnetization is greatest at 138 ppm and least at 56 ppm (Figure 6). A quantitative interpretation of this dephasing behavior requires the specification of all ^{19}F within about 6 Å of each ^{15}N. As a first approximation, we assume that the reporting HF-doped amorphous regions have chain-packing densities which are only modestly perturbed from that of crystalline-doped polyaniline.[30] A representative two-dimensional slice of this type of packing is shown in planar zig-zag form in Figure 7. We will make no attempt to specify the average orientations of the phenylene rings. The structures of Figure 7 are proposed only for amorphous regions consisting of bundles of just a few chains. Naturally, variations in spacing occur in irregularly packed amorphous regions,[31] and we will only determine an average spacing by REDOR. In addition, chain defects can occur that will drastically change the direction of local chain orientations, so that the amorphous regions have no long-range order. However, this global disorder does not affect characterization of the local ^{19}F distribution, which determines short-range ^{15}N REDOR dephasing.

We assume that the positive charge on nitrogens is not delocalized in the amorphous regions. Thus, the locations of the negatively charged fluorides cannot be inferred from those in the crystalline regions of HCl- or HBr-doped polyanilines.[30,32] Localized positive charges appear in pairs in the amorphous regions because a singly-charged imine resonance structure is unrealistic. Thus, each chain in the structure of Figure 7 consists of pairs of charged nitrogens (solid circles) alternating with pairs of uncharged nitrogens, consistent with the stoichiometric demands of full doping. In addition, each charged pair of one chain is flanked at the top and bottom by uncharged pairs from adjacent chains. This arrangement minimizes the aggregation of similar charge.

The negatively charged fluoride ions (open circles) are shown within each panel of Figure 7 in identical positions relative to the positively charged nitrogens of that panel. The fluoride position in the left panel, for example, is that of the structure associated with the low-field line assignment of Figure 3, while the position shown in the right panel is that of the structure of the high-field line assignment. (These assignments are based on our best estimates of partial charges and their effects on ^{19}F chemical shifts;[29] it is conceivable that the high- and low-field assignments should be reversed.) Mixed fluorine−nitrogen structures within a plane (that is, within a panel) have been avoided because the DRAMA and CEDRA results of Figure 5 require that isolated pairs of dipolar-coupled fluorides have the same chemical-shift environment. The two distributions of Figure 7 are not chemically identical and need not appear in equal concentrations. In fact, the greater intensity of the low-field ^{19}F line of Figure 3 (bottom) indicates that the structure of the left panel is more common than that of the right, at least at low doping levels.

If the plane on the left is shifted down by one-half chain spacing and placed above and below the plane on the right, then all charged nitrogens in the central plane will be proximate to two additional next-nearest-neighbor fluorides, one in the plane above and the other in the plane below. Fluorides in the central plane are also approximately four-coordinate with two in-plane and two out-of-plane neighboring nitrogens. This arrangement of staggered planes maximizes the proximity of dissimilar charge and has been observed in the X-ray analysis of HCl-doped polyaniline.[32] A three-plane staggered stack for the 10% HF-doped material would generate a bundle of HF-doped polyaniline chains with a 2:1 ratio of low-field to high-field ^{19}F signal intensities (see Figure 3, bottom). At higher doping levels, the low-field and high-field peaks are approximately equal in intensity, which suggests multiple planes in an alternating staggered array.

The middle peak of Figure 3 (0 Hz, arbitrary reference) is assigned to an intermediate structure in which some charge delocalization has occured. Fluorides presumably would move slightly away from the sites marked by solid circles in Figure 7 and toward the unmarked nitrogen sites. Full delocalization of charge has not occured however, and free-radical centers have not formed in the amorphous regions, possibly because of nearby structural defects.

REDOR with Multispin Dephasing. The dephasing of the ^{15}N magnetization due to the collection of nearest- and next-nearest-neighbor fluorides described above can be calculated directly, assuming that the ^{19}F spins are not coupled to each other.[33] This condition is approximately satisfied because the 6 kHz magic-angle spinning suppresses the weak homonuclear coupling between fluorines (cf., below) and the single π pulse per rotor period induces no dephasing for homonuclear coupling between spins with no isotropic chemical-shift separation (Figure 5, right). Thus, the powder average of a sum of independent dephasings (resulting from the coupling between one ^{15}N and a collection of fluorines) equals the powder average of the product of those dephasings: $S/S_0 = \langle\cos(\Sigma_i\phi_{Di})\rangle_{\text{space and spin}} = \langle\prod_i\cos(\phi_{Di})\rangle_{\text{space}}$, where ϕ_{Di} is the phase accumulation[10] resulting from the heteronuclear dipolar coupling be-

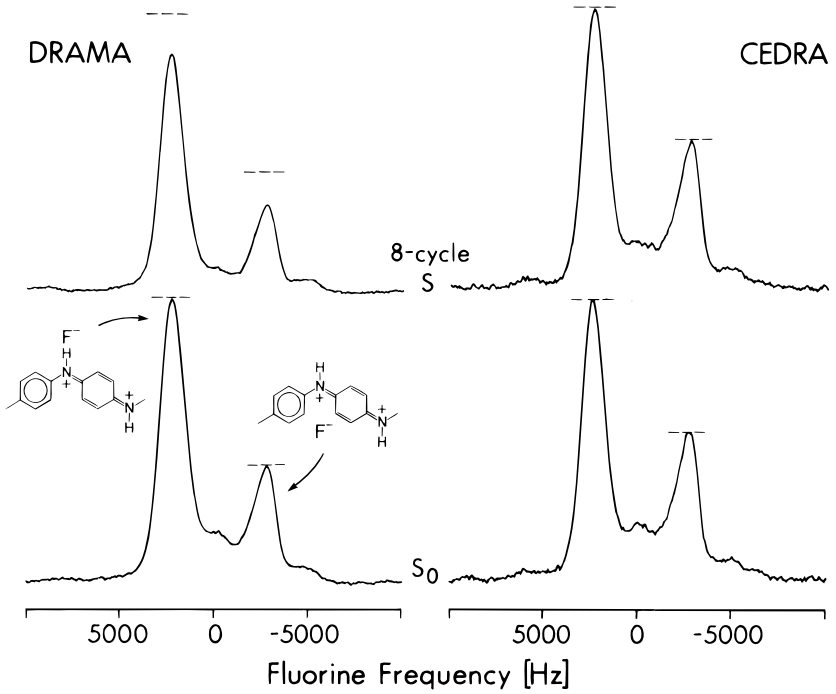

Figure 5. DRAMA (left) and CEDRA (right) ^{19}F NMR spectra of 10% HF-doped ^{15}N-labeled polyaniline after eight rotor cycles with magic-angle spinning at (left) 6250 and (right) 3333 Hz. Short T_2's have altered the relative intensities of the full-echo spectra relative to those of Figure 3 (bottom).

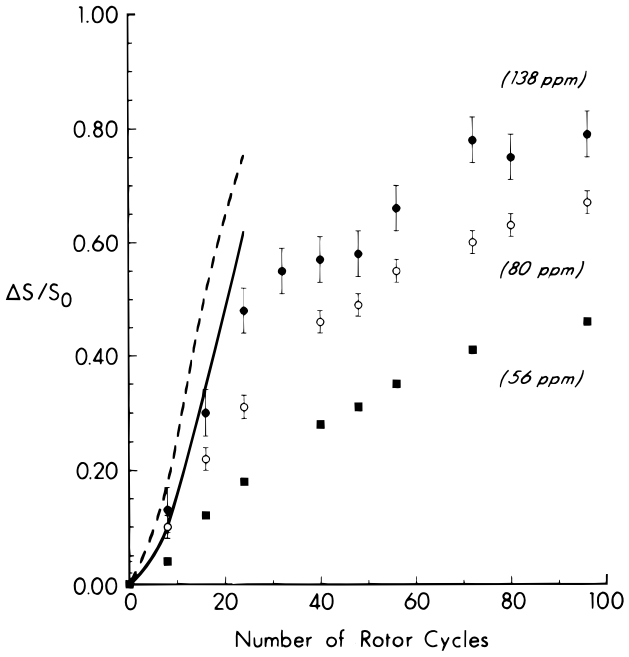

Figure 6. REDOR dephasing ($\Delta S/S_0$) at three chemical-shift positions for the HF-doped ^{15}N-labeled polyaniline of Figure 4. The solid line was calculated for a fully charged nitrogen assuming a distribution of fluorines generated by alternate staggered stacking of the planes shown in Figure 7. Each charged nitrogen had a single in-plane nearest neighbor (4.2 or 3.8 Å ^{15}N−^{19}F distances for structures associated with low- or high-field line assignments, respectively), a single in-plane next-nearest neighbor (5.5 Å), and two out-of-plane next-nearest neighbors (5.0 Å each). The dotted line was calculated assuming that the two out-of-plane ^{19}F neighbors were each 4.0 Å away.

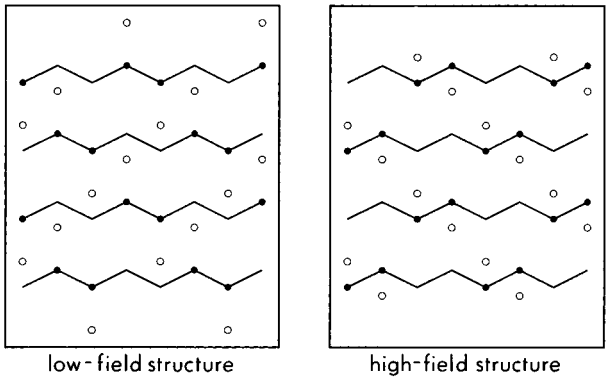

Figure 7. (LEFT) Schematic representation of a distribution of fluoride ions in a plane of fully doped polyaniline chains in which each charged nitrogen (closed circle) has one nearest-neighbor fluoride (open circle). A second fluoride next-nearest-neighbor is nearby. The nearest-neighbor fluoride position is that of the structure associated with the low-field line assignment of Figure 3. The spacing between the chains is 10 Å, the nitrogen−nitrogen distance is 5.5 Å, and the C−N−C bond angle is 140° (see ref 37). (RIGHT) Similar representation but with a location for the nearest-neighbor fluoride that corresponds to the structure of the high-field line assignment of Figure 3. If the plane on the left is shifted down by one-half chain spacing and placed above and below the plane on the right, all charged nitrogens in the central plane will be proximate to two additional next-nearest-neighbor fluorides, one in the plane above and the other in the plane below.

tween an ^{15}N and the ith fluorine, the first-angle bracket indicates an average over space and spin coordinates, and the second-angle bracket indicates just a spatial powder average. The average over spin coordinates includes dephasing by ^{15}N−^{19}F spin pairs that are parallel (positive ϕ_D) and antiparalled (negative ϕ_D) and takes advantage of the additivity of arguments for the products of exponentials.[34] This is a standard averaging procedure in SEDOR calculations for multiple dephasing spins.[35] The spatial powder average requires the specification of three Euler angles.[36]

Comparison of Calculated and Experimental REDOR Dephasing. The calculated REDOR dephasing for a fully charged nitrogen (Figure 6, solid line) is in good agreement with the experimental dephasing up to about $N_C = 24$. The solid line was calculated assuming a distribution of fluorides generated by al-

ternate staggered stacking of the planes shown in Figure 7. Each charged nitrogen was assumed to have a single in-plane nearest neighbor (4.2 or 3.8 Å $^{15}N-^{19}F$ distances[37] for structures associated with low- or high-field line assignments, respectively), a single in-plane next-nearest neighbor (5.5 Å), and two out-of-plane next-nearest neighbors (5.0 Å each). The in-plane next-nearest-neighbor distance is fixed by choice of the nearest-neighbor distance. Variation of in-plane $^{15}N-^{19}F$ distances is constrained by the need to avoid proximity of uncharged amine nitrogens and fluorides. The nearest fluoride to an uncharged amine nitrogen is about 6 Å, as determined by the amine-nitrogen $\Delta S/S_0$ of 0.2 after 24 rotor cycles (Figure 6, solid squares). This result, together with a 4 Å average distance between a fluoride and its nearest charged nitrogen, fixes the in-plane interchain separation at 10 Å. The in-plane isolated-pair $^{19}F-^{19}F$ distances are determined by the zig-zag chain geometry and the nearest-neighbor $^{15}N-^{19}F$ distances. The intraplane $^{19}F-^{19}F$ distances are 11.8 and 7.3 Å for the structures of Figure 7, left and right panels, respectively. These values are qualitatively consistent with the DRAMA dephasing results of Figure 5 (left) for the 10% HF-doped polyaniline. In these experiments, the dephasing is greater for the high-field peak, indicating a shorter intraplane $^{19}F-^{19}F$ distance. Somewhat shorter interplane $^{19}F-^{19}F$ distances could occur in fully doped materials, or 10% HF-doped material in the event of aggregation of fluorides. All of these NMR-determined $^{15}N-^{19}F$ and $^{19}F-^{19}F$ distances are averages with ±20% distributions about the averages possible.[31]

The dotted line in Figure 6 was calculated for a fully charged nitrogen assuming the two out-of-plane ^{19}F neighbors were each 4.0 Å away and is a significantly worse fit to experiment for the fully HF-doped polyaniline. We conclude that the out-of-plane next-nearest-neighbor $^{15}N-^{19}F$ distance is indeed 5.0 ± 0.5 Å, and so the interplane separation is also 5 Å. Thus, the interplane $^{19}F-^{19}F$ distance is 6.4 Å in the amorphous regions of HF-doped polyaniline, compared to the estimate of 6 Å for the corresponding distances in the crystalline domains of HCl- and HBr-doped polyanilines.[30]

Further details of the ^{19}F distribution and chain packing in HF-doped polyaniline might be extracted by comparison of experiment and theory using dephasing for $N_C > 24$, but we are reluctant to pursue this possibility at the present. The dipolar coupling for a pair of fluorines separated by 8 Å is about 600 Hz. Three-spin simulations[38] have shown that homonuclear coupling of this size diminishes heteronuclear REDOR dephasing by about 20% after 64 rotor cycles. Thus, we feel that interpretation of the dephasing behavior of Figure 7 for large ΔS exclusively in terms of $^{15}N-^{19}F$ couplings is risky. An interpretation may eventually be possible either by more elaborate multispin simulations that include at least six spins or by new experiments in which significantly faster spinning more completely suppresses the effect of the homonuclear fluorine coupling.

Acknowledgment. This work was supported by the Department of Energy OIT-AIM Program (BRM) and the Office of Naval Research (JS).

References and Notes

(1) Chiang, J.-C.; MacDiarmid, A. G. *Synth. Met.* **1986**, *13*, 193.
(2) Kaplan, S.; Conwell, E. M.; Richter, A. F.; MacDiarmid, A. G. *J. Am. Chem. Soc.* **1988**, *110*, 7647.
(3) Wudl, F.; Angus, R. O., Jr.; Lu, F. L.; Allemand, P. M.; Vachon, D. J.; Nowak, M.; Liu, Z. X.; Heeger, A. J. *J. Am. Chem. Soc.* **1987**, *109*, 3677.
(4) Epstein, A. J.; Ginder, J. M.; Zuo, F.; Bigelow, R. W.; Woo, H.-S.; Tanner, D. B.; Richter, A. F.; Huang, W.-S.; MacDiarmid, A. G. *Synth. Met.* **1987**, *18*, 303.
(5) Ginder, J. M.; Richter, A. F.; MacDiarmid, A. G.; Epstein, A. J. *Solid State Commun.* **1987**, *63*, 97.
(6) MacDiarmid, A. G.; Epstein, A. J. In *Science and Applications of Conducting Polymers*; Salaneck, W. R., Clark, D. T., Samuelson, E. J., Eds.; A. Hilger: Bristol, U.K., 1990; p 141.
(7) Anderson, M. R.; Mattes, B. R.; Reiss, H.; Kaner, R. B. *Synth. Met.* **1991**, *41*, 1151.
(8) Anderson, M. R.; Mattes, B. R.; Reiss, H.; Kaner, R. B. *Science* **1991**, *252*, 1412.
(9) Lee, P. L.; Xiao, C.; Wu, J.; Yee, A. F.; Schaefer, J. *Macromolecules* **1995**, *28*, 6477.
(10) Gullion, T.; Schaefer, J. *Adv. Magn. Reson.* **1989**, *13*, 57.
(11) McKay, R. A. U.S. Patent 4,446,431, May 1, 1984.
(12) Holl, S. M.; McKay, R. A.; Gullion, T.; Schaefer, J. *J. Magn. Reson.* **1990**, *89*, 620.
(13) Gullion, T.; Baker, D.; Conradi, M. S. *J. Magn. Reson.* **1990**, *89*, 479.
(14) Tycko, R.; Daggagh, G. *Chem. Phys. Lett.* **1990**, *173*, 461.
(15) Klug, C. A.; Zhu, W.; Merritt, M. E.; Schaefer, J. *J. Magn. Reson. A* **1994**, *109*, 134.
(16) Gullion, T.; Vega, S. *Chem. Phys. Lett.* **1992**, *194*, 423.
(17) Zhu, W.; Klug, C. A.; Schaefer, J. *J. Magn. Reson. A* **1994**, *108*, 121.
(18) Hjertberg, T.; Salaneck, W. R.; Lundstrom, I.; Somasiri, N. L. D.; Macdiarmid, A. G. *J. Polym. Sci. Polym. Lett.* **1985**, *23*, 503.
(19) Schaefer, J.; Stejskal, E. O.; McKay, R. A.; Dixon, W. T. *Macromolecules* **1984**, *17*, 1479.
(20) Garbow, J. R.; Schaefer, J. *Macromolecules* **1987**, *20*, 819.
(21) Kaplan, S.; Conwell, E. M.; Richter, A. F.; MacDiarmid, A. G. *Macromolecules* **1989**, *22*, 1669.
(22) Stein, P. C.; Earl, W. L.; Ray, A. *Synth. Met.* **1993**, *55*, 702.
(23) Adams, P. N.; Apperley, D. C.; Monkman, A. P. *Polymer* **1993**, *34*, 328.
(24) Botto, R. E.; Roberts, J. D. *J. Org. Chem.* **1979**, *44*, 140.
(25) Huang, W.-S.; Humphrey, B. D.; MacDiarmid, A. G. *J. Chem. Soc. Faraday Trans.* **1986**, *82*, 2385.
(26) Jozefowics, M. E.; Laversanne, R.; Javadi, H. H. S.; Epstein, A. J.; Pouget, J. P.; Tang, X.; MacDiarmid, A. G. *Phys. Rev. B* **1989**, *39*, 12958.
(27) Afeworki, M.; McKay, R. A.; Schaefer, J. *Macromolecules* **1992**, *25*, 4084.
(28) McBrierty, V. J.; Packer, K. J. *Nuclear Magnetic Resonance in Solid Polymers*; Cambridge University Press: Cambridge, 1993; p 191.
(29) de Dios, A. C.; Oldfield, E. *Chem. Phys. Lett.* **1993**, *205*, 108.
(30) Maron, J.; Winokur, M. J.; Mattes, B. R. *Macromolecules* **1995**, *28*, 4475.
(31) Klug, C. A.; Zhu, W.; Tasaki, K.; Schaefer, J. *Macromolecules* **1997**, *30*, 1734.
(32) Pouget, J. P.; Jozefowics, M. E.; Epstein, A. J.; Tang, X.; MacDiarmid, A. G. *Macromolecules* **1991**, *24*, 779.
(33) McDowell, L. M.; Klug, C. A.; Beusen, D. D.; Schaefer, J. *Biochemistry* **1996**, *35*, 5395.
(34) Boyce, J. B. Ph. D. Thesis, University of Illinois, Urbana-Champaign, 1972, p 28.
(35) Wang, P. K.; Slichter, C. P.; Sinfelt, J. H. *Phys. Rev. Lett.* **1984**, *53*, 82.
(36) Goetz, J. M.; Schaefer, J. *J. Magn. Reson.*, in press.
(37) Baughman, R. H.; Wold, J. F.; Eckhardt, H.; Shacklette, L. W. *Synth. Met.* **1988**, *25*, 121.
(38) McDowell, L. M.; Barkin, D.; Wilson, G. E.; Schaefer, J. *Solid State NMR* **1996**, *7*, 203.

MA970742L